High-Pressure Synthesis and Characterization of Perovskites with Simultaneous Ordering of Both the A- and B-Site Cations, $CaCu_3Ga_2M_2O_{12}$ (M = Sb, Ta)

Song-Ho Byeon,[†,⊥] Michael W. Lufaso,[§,#] John B. Parise,*[,†,‡] Patrick M. Woodward,*[,§] and Thomas Hansen[||]

Department of Geosciences and Mineral Physics Institute, and Department of Chemistry, State University of New York, Stony Brook, New York 11794, Department of Chemistry, Newman and Wolfrom Laboratory, The Ohio State University, 100 West 18th Avenue, Columbus, Ohio 43210-1185, and Institute Max von Laue and Paul Langevin, BP156, 38042 Grenoble, France

Received May 3, 2003. Revised Manuscript Received July 11, 2003

Three new perovskites, $CaCu_3Ga_2Sb_2O_{12}$, $CaCu_3Ga_2Ta_2O_{12}$, and $CaCu_3Ga_2Nb_2O_{12}$, have been synthesized at 12∼12.5 GPa and 1100 °C using the uniaxial split sphere anvil type press (USSA-2000) and recovered to ambient conditions, where they have been structurally characterized using X-ray and neutron powder diffraction. The large differences in the size and bonding preferences of Ca^{2+} and Cu^{2+} stabilize a large $a^+a^+a^+$ octahedral tilting distortion in all three compounds. This distortion creates a 12-coordinate icosahedral site for Ca^{2+} and a 4-coordinate square-planar site for Cu^{2+}. In addition to this A-site cation ordering, $CaCu_3Ga_2Sb_2O_{12}$ and $CaCu_3Ga_2Ta_2O_{12}$ also exhibit a rock salt ordering of the octahedral B-site cations. The B-site cation order decreases from 98% in $CaCu_3Ga_2Sb_2O_{12}$ to 70% in $CaCu_3Ga_2Ta_2O_{12}$ to effectively no long range order in $CaCu_3Ga_2Nb_2O_{12}$. These materials represent the first examples in which both A-site cation order and rock salt B-site cation order have been observed simultaneously. The dielectric constants of $CaCu_3Ga_2Sb_2O_{12}$ and $CaCu_3Ga_2Ta_2O_{12}$ were measured to be approximately 12 and 27, respectively, at 100 kHz. Prospects for synthesizing further perovskites exhibiting ordering of both the A- and B-site ions is evaluated using the software program SPuDS.

Introduction

Materials belonging to the perovskite structure class have attracted widespread scientific and technological interest over the past 40 years. This interest has been stimulated by perovskites which display properties such as ferroelectricity ($BaTiO_3$, $PbTiO_3$),[1] piezoelectricity ($PbZr_{1-x}Ti_xO_3$),[2] superconductivity ($BaBi_{1-x}Pb_xO_3$),[3] colossal magnetoresistance ($La_{1-x}Ca_xMnO_3$),[4] and ionic conductivity ($BaCe_{1-x}Nd_xO_{3-\alpha}$).[5] The interesting properties of perovskites originate in part from the sheer number of different compositions that crystallize with the perovskite structure. The widespread occurrence of perovskites can be attributed in large part to the flexibility of the corner-sharing octahedral framework, which allows octahedral tilting distortions to occur when the size of the A-site cation is not optimal for the octahedral framework. This feature of the perovskite topology enables a wide variety of substitutions to be carried out on either cation site. In the case of partial substitutions, ordered variants can result, and many properties are known to be very sensitive to this ordering. Distinctive ordered arrangements of the B-site cations are known for $A_2MM'X_6$ perovskites, $A_3MM'_2X_9$ perovskites, and $A_4MM'_3X_{12}$ perovskites. Ordering of the A-site cations is much less common. Layered ordering of A-site cations is observed in a few $AA'M_2X_6$ perovskites.[6] A-site cation ordering can also be stabilized by octahedral tilting distortions in $AA'_3M_4X_{12}$ perovskites.[7−9]

The most common type of ordering in perovskites occurs for a 1:1 ratio of the octahedral B-site cations, $A_2MM'O_6$ (i.e., Ba_2MgWO_6). Provided the oxidation states and radii of the two ions are not too similar, the M and M′ ions usually order onto alternating (111) planes. The M/M′ arrangement that results is es-

* Authors to whom correspondence should be addressed. E-mail: john.parise@sunysb.edu or woodward@chemistry.ohio-state.edu.
† Department of Geosciences and Mineral Physics Institute, State University of New York, Stony Brook.
‡ Department of Chemistry, State University of New York, Stony Brook.
§ Department of Chemistry, The Ohio State University.
|| Institute Max von Laue and Paul Langevin.
⊥ On leave from College of Environment and Applied Chemistry, Kyung Hee University, Kyung Ki 449-701, Korea.
Current address: Ceramics Division, National Institute of Standards and Technology, Gaithersburg, MD 20899.

(1) Elissalde, C.; Ravez, J. *J. Mater. Chem.* **2001**, *11*, 1957.
(2) Kojima, S.; Ohta, N.; Dong, X. *Jpn. J. Appl. Phys.* **1999**, *38*, 5674.
(3) Cava, R. J. *Sci. Am.* **1990**, *263*, 42.
(4) Jin, S.; Tiefel, T. H.; McCormack, M.; Fastnacht, R. A.; Ramesh, R.; Chen, L. H. *Science* **1994**, *264*, 315.
(5) Iwahara, H.; Uchida, H.; Ono, K.; Ogaki, K. *J. Electrochem. Soc.* **1988**, *135*, 529.
(6) Park, J.-H.; Woodward, P. M.; Parise, J. B. *Chem. Mater.* **1998**, *10*, 3092.
(7) Deschanvres, A.; Raveau, B.; Tollemer, F. *Bull. Soc. Chim. Fr.* **1967**, *11*, 4077.
(8) Marezio, M.; Dernier, P. D.; Chenevas, J.; Joubert, J. C. *J. Solid State Chem.* **1973**, *6*, 16.
(9) Bochu, B.; Deschizeaux, M. N.; Joubert, J. C.; Collomb, A.; Chenavas, J.; Marezio, M. *J. Solid State Chem.* **1979**, *29* , 291.

10.1021/cm034318c CCC: $25.00
Published on Web 09/13/2003

sentially a rock salt ordering of octahedra.[10] A more fragile and less common type of ordering is the 1:2 ordering that occurs in certain $A_3MM'_2O_9$ perovskites (i.e., $Ba_3ZnTa_2O_9$).[11] Because of bonding considerations at the anion site, 1:2 ordering tends to occur only when the M′ cation has an electronic configuration that allows it to shift out of the center of the octahedron. For this reason M′ is typically a d^0 cation such as Nb^{5+} or Ta^{5+}. In rare cases, the simultaneous presence of a Jahn−Teller distortion on the M′-site and the appropriate degree of octahedral tilting stabilizes layered ordering of M and M′ cations (i.e., La_2CuSnO_6).[12] Ordering of the A-site cations is much less common. The most frequently observed form of A-site cation order is stabilized by an octahedral tilting arrangement described as $a^+a^+a^+$ using Glazer's notation (i.e., $CaCu_3Ti_4O_{12}$).[9,13] In particular, $ACu_3M_4O_{12}$ perovskites favor the $a^+a^+a^+$ tilt system because Jahn−Teller Cu^{2+} cations can fully occupy square planar sites. A different pattern of A-site cation ordering can be stabilized in $AA'M_2O_6$ compounds by $a^+a^+c^-$ octahedral tilting (i.e., $CaFeTi_2O_6$),[14] but this is very rare. Layered ordering of A-site cations occurs in a few compounds provided the difference in the charge and size of the A and A′ cations is sufficiently large (i.e., $NdAgTi_2O_6$).[6] Ordering of both A- and B-site ions is very rare in compounds that are stoichiometric in oxygen. One example, $NaLaMgWO_6$, contains rock salt ordering of Mg and W in addition to layered ordering of Na and La.[15]

The A-site ordered perovskite $CaCu_3Ti_4O_{12}$ has generated a great deal of interest in recent years due to its dielectric behavior. This compound has been classified as a giant or colossal dielectric material as a result of its very large ($\epsilon_r \sim 5000$) and relatively temperature-independent (above 100 K) dielectric constant. Surprisingly the microscopic origin of this compound's unusual dielectric behavior is still not fully understood. Both intrinsic and extrinsic models have been put forward as possible explanations.[16−18] From an applications point of view it would be advantageous if the dielectric loss of $CaCu_3Ti_4O_{12}$ could be reduced. Thus far attempts to improve the dielectric properties through cation substitution on the Ca^{2+} site have not succeeded. However, among $A_2MM'O_6$ perovskites it is well-known that the dielectric properties are very sensitive to changes in the B-site cation order. Highly ordered compounds tend to have low losses (high quality factor), whereas partially ordered $Pb_2MM'O_6$ compounds have been extensively studied as relaxor ferroelectrics. Therefore, the introduction of rock salt ordering of the B-site cations into the $CaCu_3Ti_4O_{12}$ structure type offers the potential to find new materials with tunable and attractive dielectric properties. Surprisingly, there is a complete lack of any known $AA'_3M_2M'_2O_{12}$-type perovskites exhibiting simultaneous ordering on both cation sites. This challenge and the potential to find new dielectric materials led us to explore the synthesis of such perovskites using high-pressure high-temperature conditions.

Experimental Section

For the synthesis of $CaCu_3Ga_2M_2O_{12}$ (M = Sb, Ta) dried stoichiometric mixtures of $CaCO_3$, CuO, Ga_2O_3, and Sb_2O_5 or Ta_2O_5 were calcined at 900 °C in air for 8 h with intermittent grinding. The reacted oxides were then thoroughly reground and sealed in Au capsules with an inside diameter of 3.2 mm and a wall thickness of 0.1 mm. Polycrystalline samples were obtained from high-pressure treatment at 12∼12.5 GPa and 1100 °C for 3 h, followed by temperature quenching and slow decompression using the 2000-ton Uniaxial Split Sphere high-pressure apparatus (USSA 2000).[19] Details of the cell assembly along with the temperature and the pressure calibrations are described in the literature.[14,20] A typical cell assembly encapsulates the Au capsule in a MgO tube pressure medium with a graphite tube surrounding this and acting as a micro-furnace; further details are provided by Park et al.[6] for synthesis of other perovskite systems. Samples were recovered from the Au capsules as dense pellets, with each sample consisting of at least two pellets of about 50 and 25 mm^3. These pellets were used as is for neutron diffraction measurements. Cylindrical pellets for dielectric measurements with volumes of 8-9 mm^3 were obtained by sanding the faces of the pellets until level.

The initial X-ray diffraction patterns taken on the sample pellets after recovery from the high-pressure−high-temperature (HPHT) reaction were obtained using a general area detector diffraction system (GADDS) and Cu Kα radiation. Following successful synthetic runs more accurate X-ray diffraction data were collected using a small amount of sample, obtained by sanding the faces of the pellet, on a Bruker D8 Advance diffractometer, using a zero-background Si sample holder. This diffractometer was equipped with an incident beam Ge 111 monochromator and a Braun linear position sensitive detector. Rietveld refinement of X-ray powder diffraction data was carried out using the EXPGUI GSAS software package.[21,22]

Neutron powder diffraction data were collected at the high-intensity 2-axis diffractometer D20 at the ILL. The chosen setup at D20 uses a vertically focusing copper (200) monochromator in transmission ($\lambda \cong 1.29$ Å) at a takeoff angle of 42°. D20 is equipped with a micro-strip gas chamber (MSGC) position-sensitive detector (PSD), composed of 1536 separately addressed detector cells, pre-amps and amplifiers, covering 153.6° in 2θ. Data accumulate in the PSD simultaneously and this, combined with the high-flux of 10^8 $n \cdot cm^{-3} \cdot s^{-1}$ from the focusing monochromator, yields a high throughput on cm^3-sized samples. For samples from high-pressure experiments, which are of the order of 50 mm^3 in volume, the experimental setup provides data with good peak-to-background discrimination in a matter of minutes.

To obtain an optimized peak-to-background ratio for the room temperature powder diffraction patterns, the standard vacuum vessel at D20 was used to suppress background contributions from neutron air-scattering around the sample. To avoid the constant background contribution of the sample holder, we elected not to load the sample in a conventional vanadium tube. Instead the sample was laid on the edge of

(10) Wells, A. F. *Structural Inorganic Chemistry*, 5th ed.; Clarendon: Oxford, 1984.
(11) Jacobson, A. J.; Collins, B. M.; Fender, B. E. F. *Acta Crystallogr.* **1976**, *B32*, 1083.
(12) Anderson, M. T.; Poeppelmeier, K. R. *Chem. Mater.* **1991**, *3*, 476.
(13) Glazer, A. M. *Acta Crystallogra.* **1972**, *B28*, 3384.
(14) Leinenweber, K.; Parise, J. B. *J. Solid State Chem.* **1995**, *114*, 277.
(15) Sekiya, T.; Yamamoto, T.; Torii, Y. *Bull. Chem. Soc. Jpn.* **1984**, *57*, 1859.
(16) Subramanian, M. A.; Li, D.; Duan, N.; Reisner, B. A.; Sleight, A. W. *J. Solid State Chem.* **2000**, *151*, 323.
(17) Sinclair, D. C.; Adams, T. B.; Morrison, F. D.; West, A. R. *Appl. Phys. Lett.* **2002**, *80*, 2153.
(18) Homes, C. C.; Vogt, T.; Shapiro, S. M.; Wakimoto, S.; Ramirez, A. P. *Science* **2001**, *293*, 673.
(19) Liebermann, R. C.; Wang, Y. *High-Pressure Research: Application to Earth and Planery Sciences*; Terrapub: Tokyo, 1992.
(20) Gwanmesia, G. D.; Li, B.; Liebermann, R. C. *PAGEOPH* **1993**, *141*, 467.
(21) Toby, B. H. *J. Appl. Crystallogr.* **2001**, *34*, 210.
(22) Larson, A. C.; von Dreele, R. B. *General Structural Analysis System*; Los Alamos National Laboratory: Los Alamos, NM, 1994.

an absorbing cadmium sheet, vertically mounted, and inclined about 150° to the incident monochromatic neutron beam. This inclination avoids any Bragg scattering from the surface of the cadmium sheet, for diffraction angles up to the inclination angle of 150°. Thus, the resulting diffraction patterns were free from any external background contributions.

To enhance resolution, the primary divergence of the incident polychromatic neutron beam of originally 27′ has been reduced by means of a 10′ Soller collimator. To enhance further the relatively low resolution at high diffraction angles, far from the resolution optimum around the diffraction angle corresponding to the monochromator takeoff angle of 42°, the secondary divergence between monochromator and sample has been reduced by closing the horizontal monochromator aperture of 6 cm to 1 cm by means of absorbing slits close to the monochromator. Each of these modifications reduces the incident neutron flux at the sample by a factor of 4 to 5, leading to a net reduction by a factor of 20 in intensity compared to highest flux conditions. Consequently, the data collection time was increased from minutes to hours. The data for $CaCu_3Ga_2Ta_2O_{12}$ were collected during 3 h, and, as time was available, the data for $CaCu_3Ga_2Sb_2O_{12}$ were collected overnight. It is worth noting that the excellent signal-to-noise ratio that resulted leads to an $R_{expected}$ value which is extremely low, and consequently a χ^2 value which is extremely high.

Rietveld refinements of the structure were carried out simultaneously on the neutron powder diffraction and X-ray powder diffraction data using the EXPGUI GSAS software package,[21,22] except in the case of $CaCu_3Ga_2Nb_2O_{12}$ where only X-ray data was used. In the course of structurally characterizing these compounds a question arises as to the wisdom of using the X-ray and neutron data together. The neutron data is of higher quality and for the most part gives much more reliable structural parameters, but it suffers from two weaknesses. First of all, the neutron wavelength is not known nearly as accurately as the wavelength of Cu $K\alpha_1$ radiation, which will introduce errors in the unit cell dimensions and ultimately the bond distances. Second, the neutron data is not terribly sensitive to changes in the cation order parameter. In both cases use of the X-ray data markedly improves the accuracy with which these two parameters can be determined. Therefore, we feel that in this study combined refinement of the X-ray and neutron data is the best approach. Because of the very good signal-to-noise of the NPD data and the relatively poor signal-to-noise of the XRPD data the refinements are weighted more heavily in favor of the higher quality neutron data set. This is seen in the fact that the values of the atomic coordinates and displacement parameters are almost the same for refinements of NPD alone and combined refinements.

Dielectric measurements were performed using a Solartron SI 1260 impedance/gain-phase analyzer. The faces of the cylindrical pellets were sanded flat and the approximate density was determined from the mass and volume. The cylinder walls were covered with PTFE tape and the exposed ends were made conductive by gold sputtering. The pellets were placed in a sample holder between two platinum electrodes in a parallel plate capacitor arrangement. Nulling files were employed in the Zplot data collection software to reduce the contribution of the sample holder to the measurement.[23] Data were collected from 10 Hz to 10 MHz with an AC amplitude of 500 mV. Dielectric properties were obtained assuming a circuit of a capacitor and resistor in parallel in the Zview analysis software and are reported at a frequency of 100 kHz.[23]

Results

SPuDS Modeling. To narrow the compositional space to explore for possible high-pressure phases with both A- and B-site ordering we used the software program SPuDS (Structure Prediction Diagnostic Software) to generate hypothetical perovskite crystal structures.[24] SPuDS calculates ideal crystal structures of perovskites by optimizing the bond valence sums of the ions in the crystal structure. Structure optimization occurs by distorting the structure to minimize the global instability index (GII). Details of the SPuDS optimization procedure have been presented previously. The GII obtained from the SPuDS calculation is an indication of the composition stability, with a lower value indicating a more stable structure. Compositions with tilt system $a^+a^+a^+$ and a single B-site cation displayed a qualitative dependence of the reported synthesis pressure with the GII, i.e., a larger GII required higher-pressure synthetic conditions for $CaCu_3M_4O_{12}$ (M = Ge, Mn, Ru). Synthesis of $CaCu_3Ti_4O_{12}$ [SPuDS calculated GII of 0.003 valence units (v.u.)] occurs under ambient pressure, whereas for compounds in the $CaCu_3M_4O_{12}$ (M = Ge, Mn, Ru) series [SPuDS calculated GII of between 0.019 and 0.084 v.u.] high pressure is needed during the synthesis.[24]

Table 1. Global Instability Index (GII), Octahedral Δd [$d_{(M(III)-O)}$-$d_{(M(V)-O)}$] and Lattice Parameter[a]

compound	GII (v.u.)	Δd (Å)	a (Å)
$CaCu_3Cr_2Ru_2O_{12}$	0.007	−0.013	7.448
$CaCu_3Rh_2V_2O_{12}$	0.009	−0.180	7.410
$CaCu_3Ga_2Ru_2O_{12}$	0.010	−0.019	7.455
$CaCu_3Cr_2Nb_2O_{12}$	0.013	−0.002	7.461
$CaCu_3Cr_2Ir_2O_{12}$	0.016	0.003	7.467
$CaCu_3Ga_2Nb_2O_{12}$	0.016	−0.008	7.468
$CaCu_3Ga_2Ta_2O_{12}$	0.021	0.001	7.479
$CaCu_3Ga_2Sb_2O_{12}$	0.033	0.023	7.506

[a] The five structures with the lowest GII predicted by SPuDS and $CaCu_3Ga_2M_2O_{12}$ (M = Nb, Sb, Ta) are listed.

Calculations with SPuDS were used to identify $CaCu_3M^{3+}{}_2M^{5+}{}_2O_{12}$ compositions with potential to both crystallize in the $a^+a^+a^+$ tilt system, where A-site cation ordering is essentially guaranteed, and show B-site cation order. SPuDS calculations were performed for 54 combinations of compositions with $CaCu_3M^{3+}{}_2M^{5+}{}_2O_{12}$ stoichiometry. A large number of perovskite compositions were available to choose from, thus it was desired to further narrow the list of compositions by selecting the candidates most likely to undergo octahedral cation ordering. The perovksites Sr_2GaMO_6 (M = Nb, Ta) display 1:1 rock salt octahedral cation ordering.[25] In addition, the combination of Ga^{3+} and Sb^{5+} was selected, because $A_2MSb^{5+}O_6$ perovskites are almost always found to be ordered. The octahedral cation ordering observed in those compositions increases the likelihood of finding an ordered distribution of M^{3+} and M^{5+} cations in the corresponding $CaCu_3M^{3+}{}_2M^{5+}{}_2O_{12}$ compounds. The SPuDS modeling predicts that the $a^+a^+a^+$ tilt system will be the most stable perovskite configuration for the compositions listed in Table 1. The GII, lattice parameter, and the difference in the sizes of the $M^{3+}O_6$ and $M^{5+}O_6$ octahedra, Δd, are shown in Table 1 for the five compositions with the lowest GII, along with $CaCu_3Ga_2M_2O_{12}$ (M = Nb, Sb, Ta). The GII values were sufficiently small to expect that high-pressure−high-temperature synthesis techniques might stabilize

(23) ZPlot & ZView, Scribner Associates Incorporated, Southern Pines, North Carolina.

(24) Lufaso, M. W.; Woodward, P. M. *Acta Crystallogra.* **2001**, *B57*, 725.

(25) Woodward, P. M. *Ph.D Dissertation*, 1997 Oregon State University, Corvallis, OR.

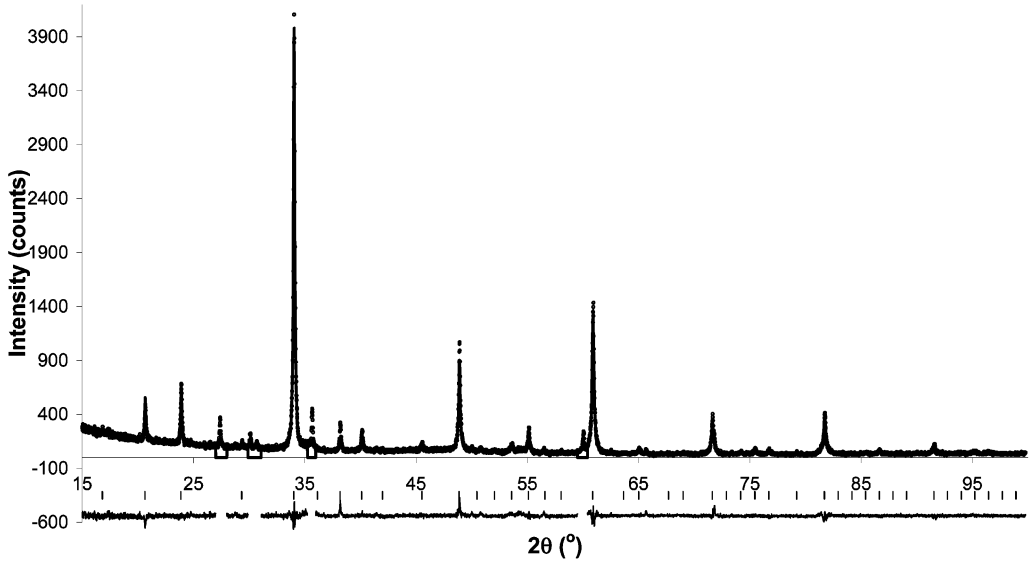

Figure 1. Observed X-ray powder diffraction data (°) along with the calculated diffraction pattern (line) obtained from Rietveld refinement of $CaCu_3Ga_2Sb_2O_{12}$. Regions of the pattern containing impurity peaks are excluded. At the bottom of the figure the difference plot ($I_{obs} - I_{calc}$) is shown. Vertical bars on the bottom indicate the positions of allowed Bragg reflections.

single-phase perovskites. The compounds with M^{5+} = Sb, Nb, and Ta were chosen as target compositions because of the relative certainty of maintaining the pentavalent oxidation state throughout the synthesis.

X-ray and Neutron Powder Diffraction. With the exception of several weak peaks from minor impurities ($I/I_{max} < 0.03$) X-ray powder diffraction patterns could be indexed on the basis of a cubic unit cell with $a \approx 7.45$ Å. Extinction conditions suggested space group symmetry $Pn\bar{3}$, consistent with an ordered perovskite structure in the $a^+a^+a^+$ Glazer tilt system.[26−28] Attempts to identify the impurity phase(s) were unsuccessful, and these trace impurities may also correspond to pressure-stabilized phases. Regions corresponding to the strongest peaks from the impurity phase(s) were excluded from subsequent Rietveld refinements when analyzing both the X-ray and neutron powder diffraction data.

Both X-ray and neutron powder diffraction data have useful characteristics with respect to carrying out accurate structural analysis of partially ordered perovskites. The strong contrast in the X-ray scattering powers of the various cations allows for an accurate determination of the site occupancy factors that are used to determine the degree of cation order. However, the X-ray scattering power of oxygen is quite small, making accurate determination of the oxide ions difficult. Yet the anion positions determine the size, tilting, and distortion of the octahedra. On the other hand, the neutron scattering length for oxygen is comparable to that of most metals, which leads to much greater accuracy in refinement of the anion positions. To get the best features of each diffraction technique we elected to carry out combined refinements using the XRPD and NPD data sets simultaneously. To get meaningful results from this approach it is necessary to allow the neutron wavelength to refine and to refine an absorption correction for the XRPD data set. During the refinements we assumed the stoichiometry $AA'_3M_2M'_2O_{12}$ with A = Ca and A′ = Cu, and Sb/Ga and Ta/Ga distributed over the B-sites such that $x^{M}_{Ga} + x^{M'}_{Ga} = 1.0$. The requirements of stoichiometry and charge balance impose constraints, which can be incorporated straightforwardly into the Rietveld refinement. In the case of $CaCu_3Ga_2Nb_2O_{12}$ the 111 reflection was absent and the peaks could be indexed on a body-centered cubic unit cell. This suggests a disordered arrangement of Ga^{3+} and Nb^{5+}, which allows us to use space group $Im\bar{3}$ for a starting model, as observed for $CaCu_3Ti_4O_{12}$. In this case we were able to refine sensible oxygen positions (0, *y*, *z*) directly from the XRPD data, and neutron data were not collected.

The oxygen atom fractional coordinates (*x*, *y*, *z*) were initially fixed at the SPuDS predicted values for the M/M′ site-ordered compounds [$CaCu_3Ga_2Sb_2O_{12}$ (0.2484, 0.4278, 0.5560), $CaCu_3Ga_2Ta_2O_{12}$ (0.2499, 0.4291, 0.5552)] and at the $CaCu_3Ti_4O_{12}$ values for the disordered $CaCu_3Ga_2Nb_2O_{12}$. The observed diffraction data, as well as the calculated pattern and difference curve from the Rietveld refinement of $CaCu_3Ga_2Sb_2O_{12}$, are shown in Figures 1 and 2. The results of the Rietveld refinements are given in Table 2. Different degrees of octahedral cation order were displayed in the compositions. A long-range order parameter can be defined with the equation $S = 2(M_M) - 1$, where M_M is the occupancy of cation M on the M site. The order parameter defined in this way can vary between 1 and 0, as the cation distribution varies from fully ordered (occupancy $M_M = 1$) to random (occupancy $M_M = 0.50$).[26] Defined in this way the long-range order parameter was observed to decrease from 98% in $CaCu_3Ga_2Sb_2O_{12}$ to 70% in $CaCu_3Ga_2Ta_2O_{12}$ to 0% in $CaCu_3Ga_2Nb_2O_{12}$. Selected interatomic distances and angles are listed in Table 3, and bond valence sums (as calculated using the bond valence parameters incorporated within SPuDS) are given in Table 4. The

(26) Woodward, P. M.; Hoffmann, R.-D.; Sleight, A. W. *J. Mater. Res.* **1994**, *9*, 2118.
(27) Aleksandrov, K. S.; Misjul, S. V. *Sov. Phys. Crystallogr.* **1981**, *26*, 612.
(28) Howard, C. J.; Kennedy, B. J.; Woodward, P. M. *Acta Crystallogr. B* **2003**, *59*, 463.

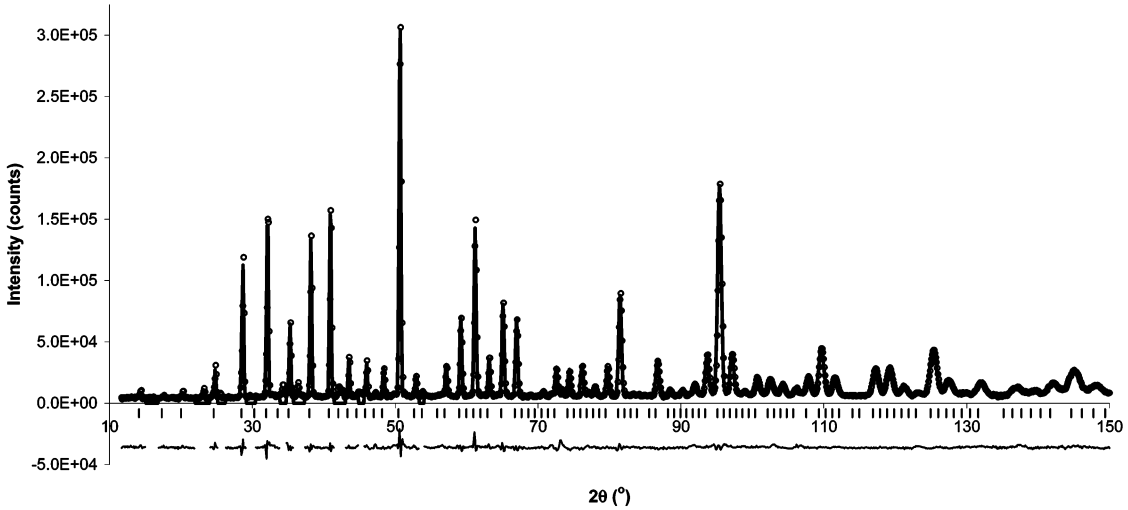

Figure 2. Observed neutron powder diffraction data (°) along with the calculated diffraction pattern (line) obtained from Rietveld refinement of $CaCu_3Ga_2Sb_2O_{12}$. Regions of the pattern containing impurity peaks are excluded. At the bottom of the figure the difference plot ($I_{obs} - I_{calc}$) is shown. Vertical bars on the bottom indicate the positions of allowed Bragg reflections.

Table 2. Rietveld Refinement Results for $CaCu_3Ga_2M'_2O_{12}$ (M′ = Sb, Ta, Nb)[a]

	M′ = Sb	M′ = Ta	M′ = Nb
Neutron Powder Diffraction Pattern			
λ (Å)	1.2956(1)	1.2957(3)	
R_{wp} %	7.52	5.99	
$R(F^2)$ %	4.79	2.93	
X-ray Powder Diffraction Pattern			
λ (Å)	1.5405	1.5405	1.5405
R_{wp} %	13.19	14.37	12.91
$R(F^2)$ %	9.77	12.40	11.03
Crystal Structure			
space group	$Pn\bar{3}$[b]	$Pn\bar{3}$[b]	$Im\bar{3}$[c]
a (Å)	7.4483(4)	7.4663(2)	7.4701(4)
M-site occupancy[d]	0.99(1) Ga 0.01 Sb	0.842(7) Ga 0.158 Ta	[e]
O(x)	0.2526(2)	0.2497(8)	0
O(y)	0.42799(9)	0.4282(1)	0.179(2)
O(z)	0.55454(8)	0.5542(1)	0.308(1)
U_{iso} (Ca) (Å^2)	0.0065(6)	0.0086(7)	0.01(1)
U_{iso} (Cu) (Å^2)	0.0057(2)	0.0059(2)	0.058(4)
U_{iso} (M) (Å^2)	0.0016(3)	0.0009(3)	0.040(2)
U_{iso} (M′) (Å^2)	0.0035(4)	0.0058(4)	0.040(2)
U_{iso} (O) (Å^2)	0.00485(9)	0.00520(8)	0.002(3)

[a] Refinements were carried out using monochromatic X-ray powder diffraction (XRPD) in the case of M′ = Nb, and combined refinements of XRPD and neutron powder diffraction (NPD) in the case of M′ = Sb, Ta. [b] $Pn\bar{3}$, Ca(2a) ($^1/_4$, $^1/_4$, $^1/_4$), Cu(6d) ($^1/_4$, $^3/_4$, $^3/_4$), M(4b) (0,0,0), M′(4c) ($^1/_2$, $^1/_2$, $^1/_2$), O(24h) (x, y, z). [c] $Im\bar{3}$, Ca(2a) (0, 0, 0), Cu(6b) (0, $^1/_2$, $^1/_2$), Ga/Nb(8c) ($^1/_4$, $^1/_4$, $^1/_4$), O(24 g) (0, x, y). [d] The occupancy of the M′ site is the inverse of the M site, so that the $CaCu_3M_2M'_2O_{12}$ stoichiometry is preserved. [e] In space group $Im\bar{3}$ the Ga and Nb atoms are disordered over a single crystallographic site.

Table 3. Selected Bond Distances (Å) and Angles(°) for $CaCu_3Ga_2M'_2O_{12}$ (M′ = Sb, Ta)[a]

	M′ = Sb	M′ = Ta
Ca−O (×12)	2.6274(7)	2.6323(8)
Cu−O (×4)	1.9691(6)	1.9764(7)
Ga−O (×6)	1.999(2)	1.981(6)
M′−O (×6)	1.961(1)	1.986(6)
O−Cu−O (×2)	84.65(4)	84.61(5)
O−Cu−O (×2)	95.36(4)	95.39(5)
O−Ga−O (×6)	89.61(3)	89.59(3)
O−Ga−O (×6)	90.39(3)	90.41(3)
O−Ga−O (×3)	180	180
O−M−O (×6)	89.68(3)	89.59(3)
O−M−O (×6)	90.32(3)	90.41(4)
O−M−O (×3)	180	180
Ga−O−M′	140.26(3)	140.40(4)

[a] From combined Rietveld refinement of X-ray and neutron powder diffraction data.

Table 4. Bond Valence Sums of the Ions in $CaCu_3Ga_2M'_2O_{12}$ (M′ = Sb, Ta)[a]

	M′ = Sb	M′ = Ta
Ca	2.01	1.99
Cu	2.07	2.03
Ga	2.90	3.04
M′	5.70	5.02
O	2.12	2.01

[a] Using bond distances from Table 3.

octahedra are quite regular, consistent with the idea of tilting of essentially rigid octahedra.

Impedance Measurements. Ideally dielectric measurements are made on dense pellets with very large surface area-to-thickness ratios. The samples made in this study have a density greater than 89% for each sample. Unfortunately, the as-synthesized cylinders are somewhat thick with a relatively small circular cross section, which is not ideal for dielectric measurements. Consequently, the measured capacitances of the $CaCu_3Ga_2M_2O_{12}$ (M = Sb, Ta) were quite small ($C < 1.0 \times 10^{-12}$ F), which is less than the measured capacitance of the open circuit sample holder. A nulling file for an open circuit sample holder was used in the data collection software in an attempt to account for the effects of the sample holder. The errors in the impedance analysis are therefore high and the values of the capacitance should be regarded with caution because of the loss of sensitivity when the nulling file becomes very important. Nonetheless, these results of these measurements, given in Table 5, clearly indicate that the dielectric constants of $CaCu_3Ga_2Sb_2O_{12}$ and $CaCu_3Ga_2Ta_2O_{12}$ are at least 2 orders of magnitude smaller than that of $CaCu_3Ti_4O_{12}$.[16] Expected dielectric constants (ϵ_{cm}) are also shown for comparison. These were calculated using the Classius-Mossotti equation and the oxide additivity rule, using published ion dielectric polarizabilities.[29,30] The polarizability of the Sb^{5+} is not given in ref. *31*. Consequently, we used a value of $\alpha(Sb^{5+}) = 3.0$ Å^3, based on unpublished measurements of other compounds

(29) Bosman, A. J.; Havinga, E. E. *Phys. Rev.* **1963**, *129*, 1593.
(30) Shannon, R. D. *J. Appl. Phys.* **1993**, *73*, 348.

Table 5. Dielectric Properties of $CaCu_3Ga_2M'_2O_{12}$ (M′ = Sb, Ta)[a]

	M′ = Sb	M′ = Ta
$\%\rho_t$	93(1)	89(1)
C ($\times 10^{-12}$ F)	0.351(2)	1.02(1)
tan δ	0.04	0.10
ϵ	11	24
ϵ_{cm}	20	39

[a] Percent of theoretical density ($\%\rho_t$), capacitance (C), loss (tan δ), relative permittivity (ϵ) and the relative permittivity calculated using the Classius−Mossotti equation (ϵ_{cm}).

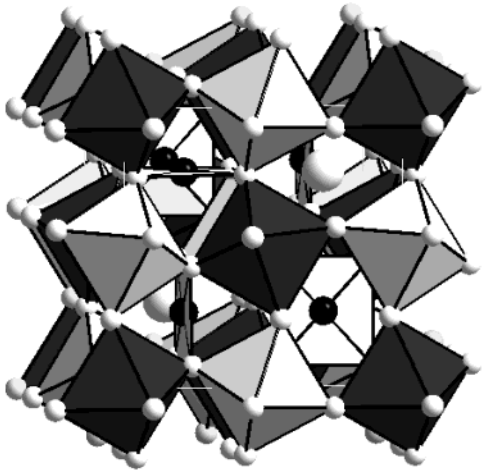

Figure 3. Idealized structure of $CaCu_3Ga_2Sb_2O_{12}$. The origin of the unit cell is at the Ga atom centered on the shaded octahedron. Large white and small dark spheres represent Ca and Cu atoms, respectively. White octahedra and small spheres represent SbO_6 octahedra and oxygen atoms, respectively.

containing Sb^{5+}. The comparison suggests that the dielectric properties of these two compounds are not out of the ordinary.

Discussion

Whereas $CaCu_3Ga_2Sb_2O_{12}$ shows essentially complete ordering of A- and B-site cations, $CaCu_3Ga_2Ta_2O_{12}$ clearly exhibits partial ordering of the B-site cations and this distribution is essentially random (on the long-range length scale) in $CaCu_3Ga_2Nb_2O_{12}$. Without in situ diffraction data it is not possible to determine if the cation distributions in these material are a result of reordering on quenching, or if they represent an equilibrium existing at the conditions of synthesis. Early indications are that variations in synthetic conditions and quench rate can vary the degree of ordering. Such behavior has been verified many times in $A_2MM'O_6$ perovskites, and is used as a tool for manipulating the physical properties. There is every reason to believe that this picture holds for HPHT synthesis as well. However, it is worth noting that the Sb and Ta members were prepared consistently with similar ordering on the A- and B-sites over a range of temperatures (1000−1200 °C), based on the relative intensity of (111).

The considerable size mismatch and differences in bonding requirements for Ca^{2+} and Cu^{2+} leads to ordering of these elements at the A-sites (Table 3, Figure 3) and to significant tilting of GaO_6 and SbO_6 octahedra. Copper is at the center of a slightly distorted square planar site (Table 3) with four next nearest oxygen atoms at about 2.8 Å and an additional four at about 3.3 Å in both the Ta and Sb-materials. Bond distances were obtained from the crystal structure determined from combined Rietveld refinement of x-ray and neutron data. The bond valence sum calculations (Table 4) show Ca, Cu, Ga, Ta, and O have near ideal values, whereas Sb is overbonded. The overbonding of the Sb^{5+} ion led us to attempt refinements where the Sb^{5+} and Ga^{3+} ions were interchanged, but in all cases the refinements gave bond distances identical to those given in Table 3. Looking into this discrepancy further we compared the octahedral cation-oxygen distances expected from bond valence sums (d(Ga−O) = 1.99 Å; d(Ta−O) = 1.99 Å; d(Sb−O) = 2.01 Å) with bond distance expectations based upon Shannon and Prewitt ionic radii (d(Ga−O) = 1.97 Å; d(Ta−O) = 1.99 Å; and d(Sb−O) = 1.95 Å).[31] The bond valence sums were calculated using SPuDS with bond valence parameters b = 0.37, $R_0(Ca^{2+}-O^{2-})$ = 1.967, $R_0(Cu^{2+}-O^{2-})$ = 1.679, $R_0(Ga^{3+}-O^{2-})$ = 1.730, $R_0(Sb^{5+}-O^{2-})$ = 1.942, and $R_0(Ta^{5+}-O^{2-})$ = 1.920.[32] Here we see that the Ga−O distance agrees somewhat better with the bond valence predictions, whereas the Sb−O distance shows noticeably better agreement with the ionic radii predictions. The structure of $CaCu_3Ga_2Sb_2O_{12}$, as well as Sb^{5+}−O distances seen in other perovskites, suggest that the bond valence parameter for this bond should be reinvestigated. The experimentally observed Ta−O distances are in excellent agreement with the predictions of both methods. The smaller size of Sb^{5+}, in comparison to that of Ta^{5+}, is consistent with the fact that the smallest unit cell volume among the $CaCu_3Ga_2M'_2O_{12}$ compounds is observed when M′ = Sb^{5+}.

Conclusions

The software program SPuDS was successfully utilized to predict the stability of dual A- and B-site cation ordered perovskites in the $a^+a^+a^+$ tilt system. Three new compounds, $CaCu_3Ga_2M_2O_{12}$ (M = Sb, Ta, Nb), were successfully synthesized under high-pressure−high-temperature conditions with minor impurities. $CaCu_3Ga_2Sb_2O_{12}$ possesses essentially complete order on both the A- and B-cation sites, whereas $CaCu_3Ga_2Ta_2O_{12}$ shows partial B-site cation order and $CaCu_3Ga_2Nb_2O_{12}$ exhibits a disordered B-site cation distribution. Structure refinements using X-ray and neutron data indicate a close correspondence between predicted and observed structures. The porosity-corrected[33] dielectric constants (M′ = Sb, ϵ = 12; M′ = Ta, ϵ = 27) show reasonable agreement with the values expected from the oxide additivity rule and the Clausius-Mossotti equation (M′ = Sb, ϵ = 20; M′ = Ta, ϵ = 39).

Many additional compositions are predicted by SPuDS to be stable under high-pressure−high-temperature synthetic conditions similar to those used in this study. Thus, there is every reason to expect that these compounds represent the first of many $AA'_3M_2M'_2O_{12}$ compositions with dual cation ordering. A systematic examination of structural and dielectric properties of

(31) Shannon, R. D. *Acta Crystallogr.* **1976**, *A32*, 751.
(32) Accumulated Table of Bond Valence Parameters version 2.2, http://www.ccp14.ac.uk/ccp/web-mirrors/i_d_brown/ (Accessed April 2003).
(33) Geyer, R. G.; Barker-Jarvis, J.; Vanderah, T. A.; Mantese, J. *Advances in Dielectric Ceramic Materials*; American Ceramic Society: Westerville, OH, 1998; pp 115−128.

additional compositions will perhaps provide insight into the giant dielectric constant $CaCu_3Ti_4O_{12}$ and enrich the understanding of the structural chemistry of $Pn\bar{3}$ perovskites.

Acknowledgment. Research carried out at Stony Brook was supported by grants NSF-DMR-0095633 and EAR-0125094. Research carried out at Ohio State was supported by the National Science Foundation grant # DMR-0094271.

Supporting Information Available: Crystallographic information for the subject perovskites (CIF). This material is available free of charge via the Internet at http://pubs.acs.org.

CM034318C